



# Phase transition in $\text{MgSiO}_3$ perovskite in the earth's lower mantle

Taku Tsuchiya\*, Jun Tsuchiya, Koichiro Umemoto, Renata M. Wentzcovitch

*Department of Chemical Engineering and Materials Science, Minnesota Supercomputing Institute for Digital Technology and Advanced Computations, University of Minnesota, 421 Washington Av. SE, Minneapolis, MN 55455, USA*

Received 26 April 2004; received in revised form 28 April 2004; accepted 11 May 2004

## Abstract

A new polymorph of  $\text{MgSiO}_3$  more stable than the  $Pbnm$ -perovskite phase has been identified by first-principles computations. It has the  $\text{CaIrO}_3$  structure with  $Cmcm$  symmetry and consists of  $\text{SiO}_3$  layers intercalated by eightfold-coordinated Mg ions. High-temperature calculations within the quasiharmonic approximation give a volume change of  $\sim 1.5\%$  and a Clapeyron slope of  $\sim 7.5 \pm 0.3$  MPa/K at  $\sim 2750$  K and  $\sim 125$  GPa. These pressure–temperature ( $P$ – $T$ ) conditions are close to those in which a phase transition in  $\text{MgSiO}_3$ -perovskite has been observed by in situ angle dispersive X-ray diffraction measurements. This transition appears to be associated with the  $D''$  discontinuity.

© 2004 Elsevier B.V. All rights reserved.

**Keywords:** post-perovskite;  $\text{MgSiO}_3$ ; first principle; core–mantle boundary;  $D''$  layer

## 1. Introduction

The high-pressure  $Pbnm$ -perovskite polymorph of  $\text{MgSiO}_3$  [1] is believed to be the most abundant mineral in the earth's lower mantle [2]. The possibility of a phase transition in this polymorph has been controversial for several years. Reports of its dissociation into  $\text{SiO}_2$  and MgO at 70–80 GPa and 3000 K [3,4], or of a possibly subtle phase change above 83 GPa and 1700 K [5], or of no phase transition at all [6] up to 94 GPa and 2500 K, have appeared in the literature. Although the pressure–temperature ( $P$ – $T$ ) conditions in these experiments were quite high, none

of them had reached the conditions expected in the  $D''$  region. Recently, a drastic change in the X-ray diffraction of perovskite, suggesting a radical structural change, was observed at 125 GPa and 2500 K [7], and, more recently, the post-perovskite crystal structure was reported [8]. Understanding of the post-perovskite transition and of the properties of the post-perovskite phase is essential for a better understanding of the deep lower mantle, particularly of the  $D''$  region [9–13]. Here we show through first-principles high  $P$ – $T$  computations that a structural transition occurs in  $Pbnm$ -perovskite.

## 2. The post-perovskite structure

The techniques used here and the details of this calculation are similar to those used in previous high  $P$ – $T$  calculations of the  $Pbnm$ -perovskite phase [14].

\* Corresponding author. Tel.: +1-612-625-8597; fax: +1-612-626-7246.

*E-mail addresses:* [takut@cems.umn.edu](mailto:takut@cems.umn.edu) (T. Tsuchiya), [junt@cems.umn.edu](mailto:junt@cems.umn.edu) (J. Tsuchiya), [umemoto@cems.umn.edu](mailto:umemoto@cems.umn.edu) (K. Umemoto), [wentzcov@cems.umn.edu](mailto:wentzcov@cems.umn.edu) (R.M. Wentzcovitch).

Computations were performed using the local density approximated (LDA) [15,16] and the generalized gradient approximation (GGA) [17]. Pseudopotentials for oxygen and silicon were generated by the methods of Troullier and Martins [18]. The cutoff radii are: (a) for oxygen in the configuration  $2s^2 2p^4$ ,  $r(2s)=r(2p)=1.45$  a.u., with p nonlocality; (b) for silicon in the configuration  $3s^2 3p^4 3d^0$ ,  $r(3s)=1.47$  a.u.,  $r(3p)=1.47$  a.u.,  $r(3d)=1.47$  a.u., with d nonlocality. The method of von Barth and Car [19] was used for magnesium. Five configurations,  $3s^2 3p^0$ ,  $3s^1 3p^1$ ,  $3s^1 3p^{0.5} 3d^{0.5}$ ,  $3s^1 3p^{0.5} 3s^1 3d^1$  with decreasing weights 1.5, 0.6, 0.3, 0.3, and 0.2, respectively, were used. Cutoff radii were  $r(3s)=$

$r(3p)=r(3d)=2.5$  a.u. with d nonlocality. The plane wave energy cutoff was 70 Ry. Brillouin zone sampling for electronic states (phonons) was carried out on 6 (14) and 2 special (18) k-points (q-points) for the perovskite and post-perovskite phases, respectively. Phonon frequencies were obtained using density functional perturbation theory [20,21]. Structural searches were performed using variable cell shape molecular dynamics [22]. Thermodynamic properties were determined using the quasiharmonic approximation [23]. Computations were performed with the PWscf code [24].

The search for the post-perovskite structure was guided by two general principles: (a) polyhedron

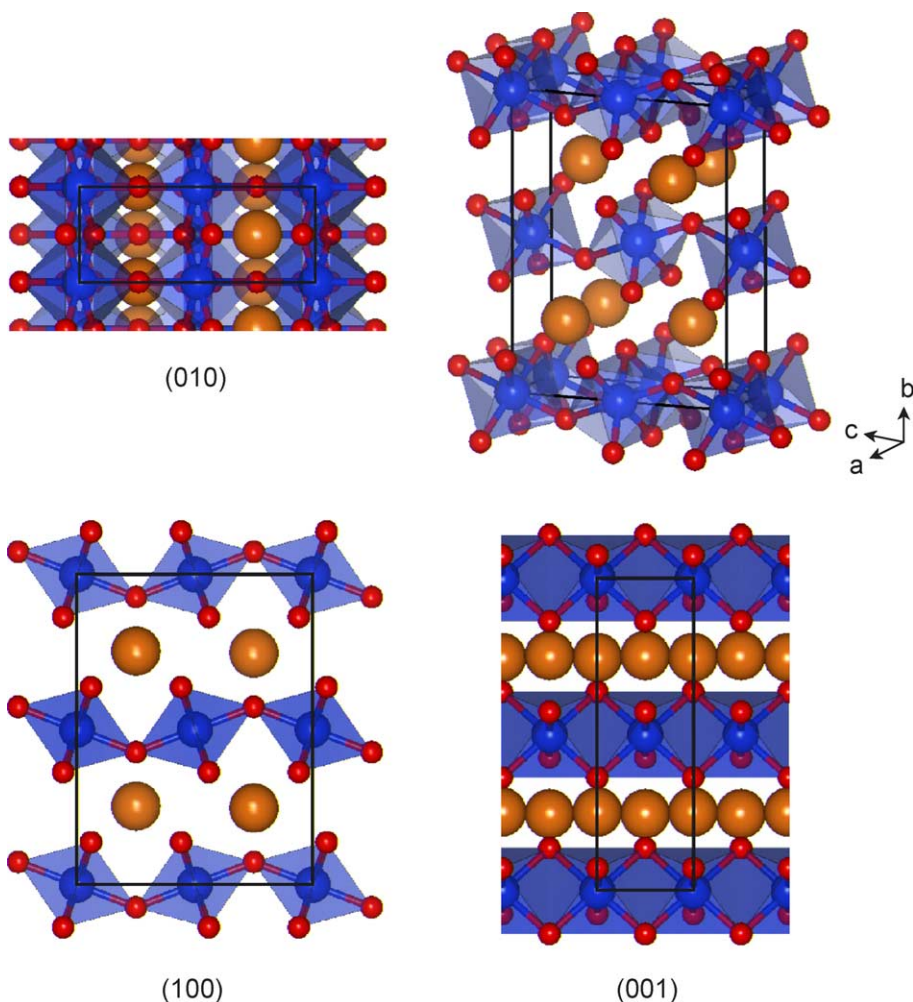


Fig. 1. The  $Cmc21$  post-perovskite crystal structure. Blue, orange, and red spheres represent Si, Mg, and O ions, respectively.

types and interconnections that would be reasonable at ultrahigh pressures; and (b) extrapolation of the compressive mechanism of the *Pbnm*-perovskite structure. Edge-sharing rutile-like columns form a more compact octahedral arrangement, but the stoichiometry requires these columns to be connected by the octahedral apices. This produces the  $\text{SiO}_3$  layers. These layers should then be intercalated by magnesium ions with the highest possible coordination. These criteria produce a family of structures. After exploring more than 30 prototypes, we found, independently, this one shown in Fig. 1. All attempted structures were fully optimized above 120 GPa using variable cell shape damped molecular dynamics [22], and their enthalpies were then compared with *Pbnm*-perovskite's. The structure in Fig. 1 is the only one we found with lower enthalpy than perovskite in static LDA [15,16] and/or generalized gradient approximation (GGA) [17] calculations. This is the structure of  $\text{CaIrO}_3$  [25], the same one found by Murakami et al. [8]. This structure is base-centered orthorhombic with space group *Cmcm*. Magnesium ions are located in approximately eightfold-coordinated sites, at the center of irregular hendecahedra. Like the *Pbnm*-perovskite structure, it has four formulae unit per

conventional cell ( $Z=4$ ), but it is very anisotropic. Static isotropic compression using LDA revealed a transition pressure of  $98 \pm 3$  GPa ( $109 \pm 4$  GPa using the GGA).

The relationship between this *Cmcm* and the *Pbnm* structures can be understood on the basis of the extrapolated compressive behavior of  $\text{MgSiO}_3$ -perovskite [26]. The angles between the octahedral edges bisected by the (110) plane in the *Pbnm* structure (see Fig. 2) decrease faster than other similar angles. The *Cmcm* structure can be produced by forcing these angles to close faster under strain  $\epsilon_6$ . Fig. 2 shows structures that result by applying strains  $\epsilon_6$  in the *Pbnm*-perovskite first equilibrated at 120 GPa. For sufficiently large strains, these angles vanish and form edge-sharing rutile columns when one of the oxygens in each pair of edges defining these angles is removed. This process forces layer formation. In the third direction, perpendicular to the columns and to the layers, octahedra remain connected at the apices. According to this transition mechanism, the  $[100]_{\text{ppv}}$ ,  $[010]_{\text{ppv}}$ , and  $[001]_{\text{ppv}}$  directions in the *Cmcm* structure correspond to the  $[1\bar{1}0]_{\text{pv}}$ ,  $[110]_{\text{pv}}$ , and  $[001]_{\text{pv}}$  in the *Pbnm* structure, respectively. Structural parameters obtained in static LDA calculations at 120 GPa are given in

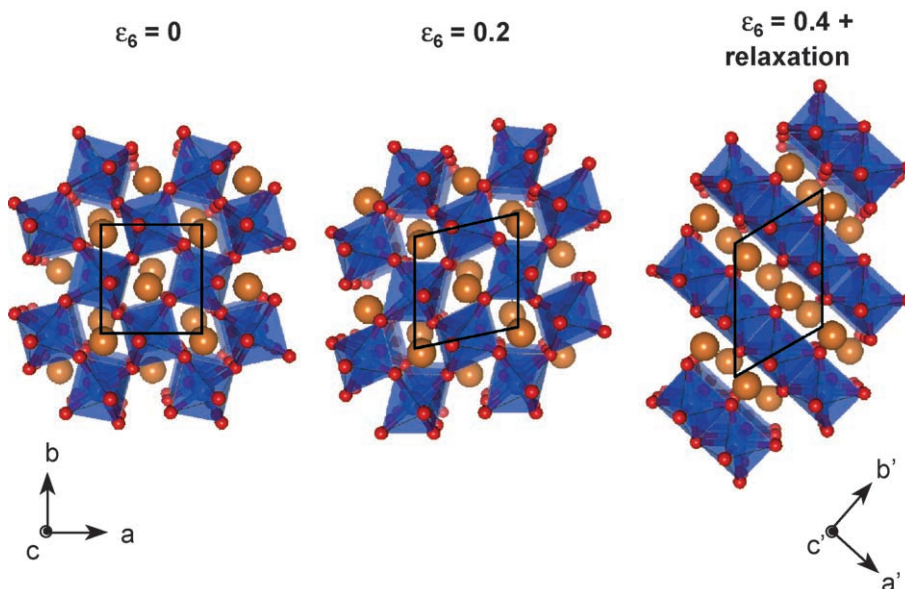


Fig. 2. Relaxed (optimized) *Pbnm*-perovskite structure at 120 GPa under shear strain  $\epsilon_6$ . Following the relaxation of internal degrees of freedom with  $\epsilon_6=0.4$ , a complete relaxation was performed.

Table 1

Structural parameters and equation of state parameters of *Cmcm* post-perovskite and *Pbnm* perovskite

Space group	<i>Cmcm</i>			
	Base-centered orthorhombic			
Formula unit (Z)			4 (4)	
Cell dimensions (Å)	<i>a</i>		2.462 (4.286)	
	<i>b</i>		8.053 (4.575)	
	<i>c</i>		6.108 (6.268)	
Atomic coordinates	Wyckoff position	<i>x</i>	<i>y</i>	<i>z</i>
Mg	4c (4c)	0 (0.525)	0.253 (0.578)	3/4 (1/4)
Si	4a (4b)	0 (1/2)	0 (0)	0 (0)
O1	4c (4c)	0 (0.117)	0.073 (0.467)	1/4 (1/4)
O2	8f (8d)	0 (0.182)	0.363 (0.192)	0.441 (0.557)
Bond distances (Å)	Mg–O		1.865 × 2, 1.936 × 4, 2.084 × 2	
			(1.821 × 1, 1.853 × 2, 1.881 × 1, 2.031 × 2, 2.187 × 2)	
	Si–O		1.636 × 2, 1.692 × 4 (1.651 × 2, 1.653 × 2, 1.661 × 2)	
Polyhedral volume (Å <sup>3</sup> )	Mg		24.04 (24.66)	
	Si		6.23 (6.06)	
Bulk modulus (GPa)	<i>B</i> <sub>0</sub>		222(1) (248(1))	
	<i>dB/dP</i>		4.2(1) (3.91(1))	
Ambient volume (cm <sup>3</sup> /mol)	<i>V</i> <sub>0</sub>		24.662(7) (24.704(4))	
Grüneisen parameter	$\gamma_0$		1.64 (1.53)	
	$(\partial \ln \gamma / \partial \ln V)_T$		−0.27 + 2.13( <i>V/V</i> <sub>0</sub> ) (0.32 + 0.86( <i>V/V</i> <sub>0</sub> ))	
Debye temperature (K)	$\Theta_0$		1100 (1114)	

Cell dimensions, atomic coordinates, and bond distances were obtained in static LDA optimizations at 120 GPa. All EoS parameters are at 300 K and zero pressure. Uncertainties in these parameters include the range of values obtained by fitting third-order finite strain and Vinet et al. [27] EoSs. The Debye temperature was estimated by fitting the specific heat to the Debye model. Values for perovskite are in parentheses.

Table 1. The inset in Fig. 4B shows the pressure dependence of the *b/a* and *c/a* ratios in this phase as obtained from static calculations. As expected, the structure is more compressible along [010].

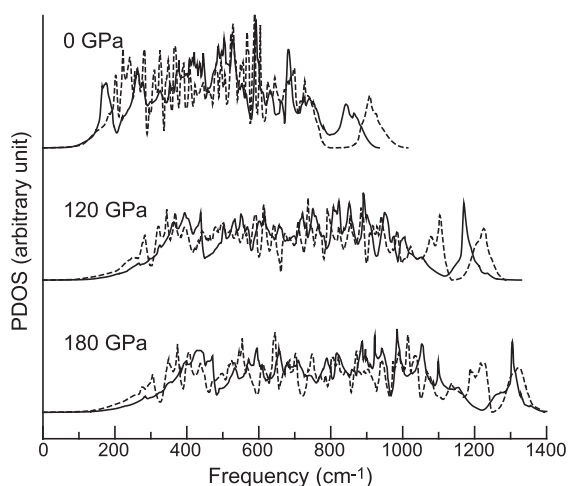


Fig. 3. Vibrational densities of state for perovskite (dashed) and post-perovskite (full).

### 3. Thermodynamic properties and phase equilibrium

We then proceeded with calculations of phonon dispersions and vibrational densities of states (VDOS) (see Fig. 3) to obtain Gibbs free energies within the QHA. Finite temperature equation of state (EoS) parameters is also summarized in Table 1. The uncertainties in these parameters represent the range of values obtained by fitting third-order finite strain and Vinet et al. [27] EoSs. At 300 K, the zero-pressure bulk modulus,  $B_0 = 221(1)$  GPa, is substantially smaller than perovskite's, 248(1) GPa. However, the pressure derivative of the bulk modulus,  $B' = 4.2(1)$ , is distinctly larger than perovskite's, 3.91(1). The zero-pressure Grüneisen parameter,  $\sim 1.6$ , and the Debye temperature,  $\Theta_D \sim 1100$  K, are fairly comparable to those of perovskite. Comparison between the volumes of both phases at the same  $P$ – $T$  conditions indicates that the post-perovskite phase is always denser than the perovskite (see Fig. 4B).

LDA and GGA calculations including zero-point motion tend to overestimate equilibrium volumes and

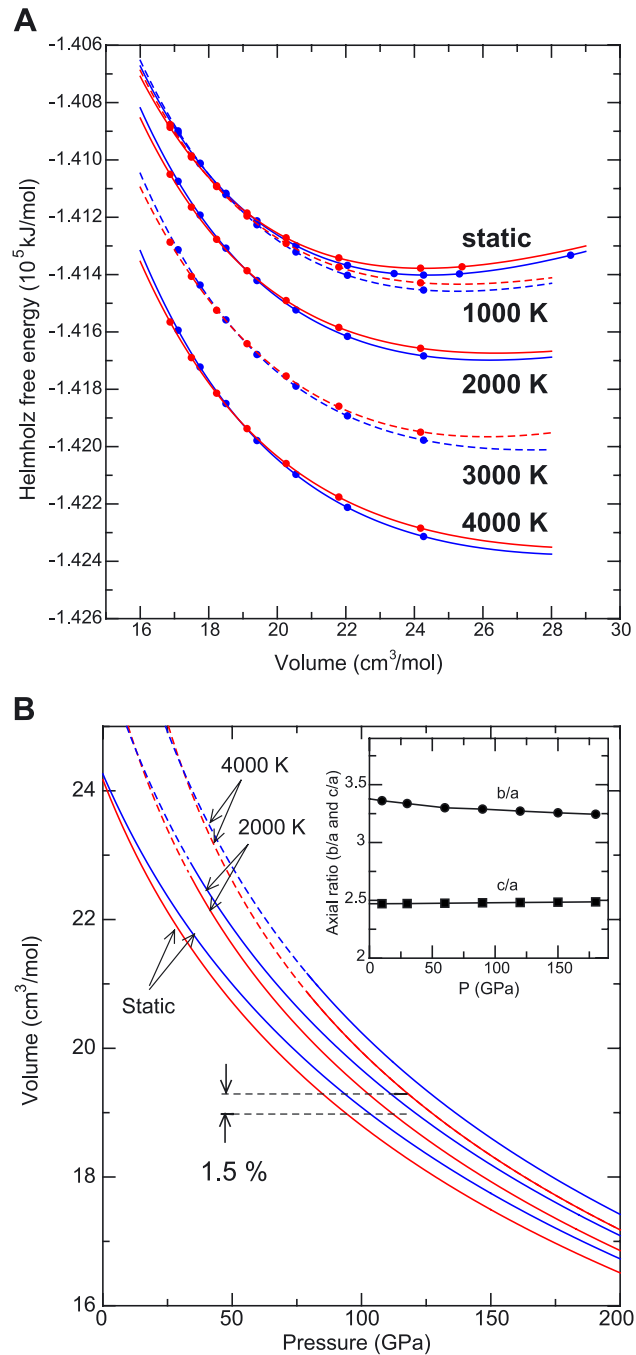


Fig. 4. (A) Helmholtz free energy versus volume at various temperatures for perovskite (blue) and post-perovskite (red) and (B) calculated compression curves of perovskite (blue) and post-perovskite (red). Dashed lines in (B) correspond to conditions where the validity of the QHA is questionable.

underestimate bulk moduli, with deviations being smaller with the former (see [14] and references therein). However, there is little experience with the effect of these systematic deviations and with the use of the QHA on calculated transition pressures. A recent detailed LDA calculation of the akimotoite-to-perovskite transition in  $\text{MgSiO}_3$  [28] indicated that transition pressures with LDA are underestimated by  $\sim 5$  GPa and the Clapeyron, negative one in that case, is overestimated. The main source of these deviations is the description of the exchange correlation energy in density functional theory. In static calculations, LDA tends to underestimate transition pressures and GGA results are usually in better agreement with experiments. The inclusion of zero-point motion in the calculation of a phase boundary with positive Clapeyron slope shifts the boundary to higher pressures [28],  $\sim 2$  GPa in this case. It is therefore reasonable to anticipate that the true transition pressure falls between the phase boundaries given by LDA and GGA. Direct comparison of the Gibbs free energies of both phases produces the phase boundary shown in Fig. 5. The width represents the range of values obtained using the LDA (left bound) and the GGA (right bound). Intermediate values for the transition pressures are expected to be more realistic. Indeed, these values are closer to Murakami's estimation of the phase boundary position [7,8]. However, there are also large uncertainties associated with the platinum scale in this  $P$ – $T$  range [29,30]. It tends to overestimate pressure by  $\sim 10$  GPa when compared with the gold scale [31]. The Clapeyron slope at 2500 K is  $\sim 7.5 \pm 0.3$  MPa/K.

#### 4. Geophysical significance

This transition is important for understanding the state of the deep lower mantle, particularly that of the  $D''$  region, at the bottom 300 km [9–13]. The  $D''$  layer has wide topography [10] and is quite anisotropic [12]. Chemical heterogeneity, partial melting, phase transitions, preferred orientations, or a combination of all of these have been proposed as possible mineralogical origins of these features. In particular, it has been argued on the basis of seismic and geodynamic considerations that a solid–solid phase changes with a Clapeyron slope of  $\sim 6$  MPa/K [9] could cause the

observed topography. Our Clapeyron slope of  $7.5 \pm 0.3$  MPa/K is quite close to this value. The presence of alloying elements, such as aluminum and iron, is likely to affect the transition pressure and the Clapeyron slope, particularly if minor element partitioning between  $\text{MgSiO}_3$  and other coexisting phases is affected. For instance, silicon and magnesium polyhedral volumes increase and decrease, respectively, across the transformation (see Table 1). This might affect element partitioning. It suggests also that aluminum- or aluminum- and iron-(III)-bearing perovskite [perovskite with coupled  $(\text{Al}^{3+}, \text{Al}^{3+})$  or  $(\text{Al}^{3+}, \text{Fe}^{3+})$  substitution for  $(\text{Mg}, \text{Si})$ ] should transform at lower pressures, while iron-(II)-bearing perovskite ( $\text{Fe}^{2+}$  substitution for  $\text{Mg}^{2+}$ ) might transform at higher pressures, maybe accompanied by a high- to low-spin transition in iron, as happens in ferroperrichase [32] ( $\text{Fe}^{2+}$  is “larger” in the high-spin state configuration). The structural relationship between the  $Pbnm$  and the  $Cmcm$  phases found here suggests that also shear stresses are likely to affect the transition pressure (in both directions). Shear stresses are expected particularly near the CMB. Also, the possibility of an intervening perovskite phase with different symmetry as suggested by Shim et al. [5], could increase the post-perovskite transition pressure.

Across the  $D''$  topography, pressure varies from  $\sim 125$  to  $\sim 133$  GPa. This is indicated in Fig. 5 by the vertical semitransparent gray band. Our best estimate of the transition temperature in pure  $\text{MgSiO}_3$ -perovskite through this pressure range is  $2750$ – $3800 \pm 250$  K. These temperatures are consistent with the existence of a post-perovskite transition before the core–mantle boundary where temperatures can reach  $\sim 4100$  K [33,34] and point to the possibility of 1000 K lateral temperature variations in this region. However, the effect of composition, stress state, and of a possible intervening perovskite structure [5] on this transition still must be investigated before an attempt is made to relate the  $D''$  topography and lateral temperature variations through the post-perovskite transition.

The layered post-perovskite structure is potentially very anisotropic. Although reaction products between molten iron and  $\text{MgSiO}_3$ , such as  $\text{FeSi}$ ,  $\text{FeO}$ ,  $\text{SiO}_2$ , and  $\text{FeO}$ , are anticipated to co-exist in this region, in addition to an accumulation of light elements from the core,  $\text{MgSiO}_3$ -post-perovskite might be the most abundant phase in  $D''$ , and preferred orientation in

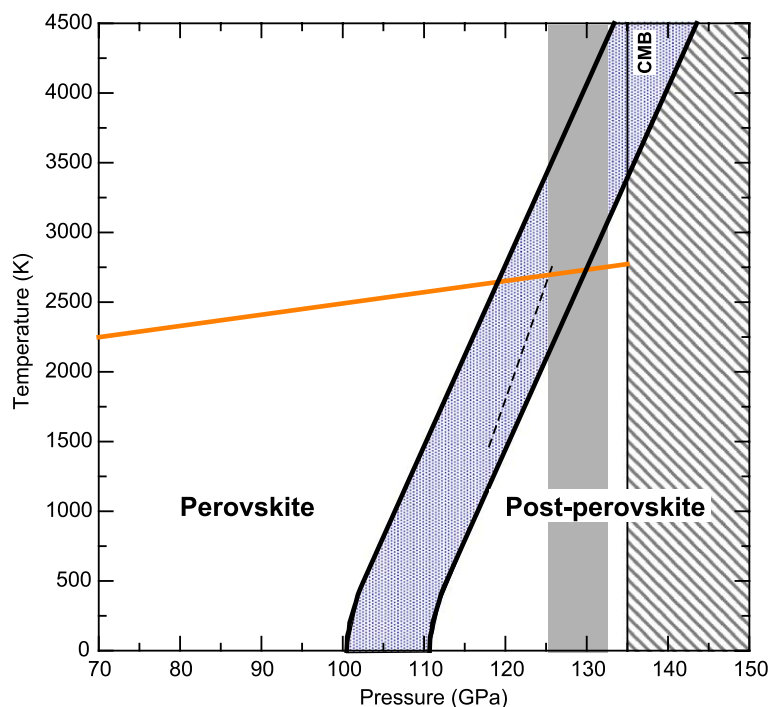


Fig. 5. Phase boundary for this transition using the QHA. The bound was determined from LDA calculations and the upper bound from GGA. Intermediate values are expected to be more realistic. The dashed line is the phase boundary proposed in [9]. The orange line is the mantle geotherm [35]. The vertical gray band is the pressure range across the  $D''$  topography [9].

this structure is an additional potential source of anisotropy in this region.

## 5. Conclusion

A new polymorph of  $\text{MgSiO}_3$  with the  $\text{CaIrO}_3$  structure and more stable than the  $Pbnm$ -perovskite phase has been identified by first-principles computations. The  $\text{CaIrO}_3$  structure is shown to be related with the  $Pbnm$ -perovskite structure through a shear strain  $\epsilon_6$ . This structural relationship suggests that the post-perovskite phase transition pressure might be affected by shear stresses. Quasiharmonic high-temperature calculations of the thermodynamic phase boundary gives a Clapeyron slope of  $\sim 7.5 \pm 0.3$  MPa/K at  $\sim 2750$  K and  $\sim 125$  GPa. These  $P$ – $T$  conditions are close to those anticipated in the  $D''$  region and this Clapeyron slope is close to that anticipated if the  $D''$  topography were related to a solid–solid transformation. Our results suggest that the post-perovskite

transition might be associated with the  $D''$  discontinuity and that this layered polymorph might provide an additional source of anisotropy in the  $D''$  region.

## Acknowledgements

The authors thank K. Hirose and M. Murakami for supplying experimental data and D. Yuen, M. Akaogi, K. Fujino, E. Ito, and K. Takemura for helpful comments. This research was supported by NSF/EAR 0135533 and 0230319. T.T. and J.T. acknowledge the Japan Society for the Promotion of Science (JSPS) for research fellowships. [SK]

## References

- [1] L.-G. Liu, Silicate perovskite from phase transformations of pyrope-garnet at high pressure and temperature, *Geophys. Res. Lett.* 1 (1974) 277–280.

- [2] E. Knittle, R. Jeanloz, Synthesis and equation of state of (Mg, Fe)SiO<sub>3</sub> perovskite to over 100 gigapascals, *Science* 235 (1987) 668–670.
- [3] C. Meade, H.K. Mao, J. Hu, High-temperature phase transition and dissociation of (Mg, Fe)SiO<sub>3</sub> perovskite at lower mantle pressures, *Science* 268 (1995) 1743–1745.
- [4] S.K. Saxena, L.S. Dubrovinsky, P. Lazor, Y. Cerenius, P. Häggkvist, M. Hanfland, J. Hu, Stability of perovskite (MgSiO<sub>3</sub>) in the earth's mantle, *Science* 274 (1996) 1357–1359.
- [5] S.-H. Shim, T.S. Duffy, G. Shen, Stability and structure of MgSiO<sub>3</sub> perovskite to 2300-kilometer depth in earth's mantle, *Science* 293 (2001) 2437–2440.
- [6] G. Fiquet, A. Dewaele, D. Andrault, M. Kunz, T. Le Bihan, Thermoelastic properties and crystal structure of MgSiO<sub>3</sub> perovskite at lower mantle pressure and temperature conditions, *Geophys. Res. Lett.* 27 (2000) 21–24.
- [7] M. Murakami, K. Hirose, N. Sata, Y. Ohishi, preprint (2003).
- [8] M. Murakami, K. Hirose, K. Kawamura, N. Sata, Y. Ohishi, Post-perovskite phase transition in MgSiO<sub>3</sub>, *Sci. Express* 304, 855–858.
- [9] I. Sidorin, M. Gurnis, D.V. Helmberger, Evidence for a ubiquitous seismic discontinuity at the base of the mantle, *Science* 286 (1999) 1326–1331.
- [10] T. Lay, D.V. Helmberger, A lower mantle S wave triplication and the shear velocity structure of D'', *Geophys. J. R. Astron. Soc.* 75 (1983) 799–838.
- [11] T. Lay, Q. Williams, E.J. Garnero, The core–mantle boundary layer and deep earth dynamics, *Science* 392 (1998) 461–468.
- [12] M.E. Wysession, T. Lay, J. Revenaugh, Q. Williams, E.J. Garnero, R. Jeanloz, L.H. Kellog, Implications of the D'' discontinuity, in: M. Gurnis, M.E. Wysession, E. Knittle, B. Buffett (Eds.), *The Core–Mantle Boundary Region*, Geodynamic Series. vol. 28, American Geophysical Union, Washington, DC, 1998, pp. 273–297.
- [13] M.E. Wysession, A. Langenhorst, M.J. Fouch, K.M. Fischer, G.I. Al-Eqabi, P.J. Shore, T.J. Clarke, Lateral variations in compressional/shear velocities at the base of the mantle, *Science* 284 (1999) 120–124.
- [14] R.M. Wentzcovitch, B.B. Karki, M. Cococcioni, S. de Gironcoli, Thermoelastic properties of MgSiO<sub>3</sub> perovskite: insights on the nature of earth's lower mantle, *Phys. Rev. Lett.* 92 (2004) 018501.
- [15] D. Ceperley, B. Alder, Ground state of the electron gas by a stochastic method, *Phys. Rev. Lett.* 45 (1980) 566–569.
- [16] J. Perdew, A. Zunger, Self-interaction correction to density-functional approximations for many-electron systems, *Phys. Rev., B* 23 (1981) 5048–5079.
- [17] J.P. Perdew, K. Burke, M. Ernzerhof, Generalized gradient approximation made simple, *Phys. Rev. Lett.* 77 (1996) 3865–3868.
- [18] N. Troullier, J.L. Martins, Efficient pseudopotentials for plane-wave calculations, *Phys. Rev., B* 43 (1991) 1993–2006.
- [19] U. von Barth, R. Car, (unpublished).
- [20] S. Baroni, P. Giannozzi, A. Testa, Green's function approach to linear response in solids, *Phys. Rev. Lett.* 58 (1987) 1861–1864.
- [21] P. Giannozzi, S. de Gironcoli, P. Pavone, S. Baroni, Ab initio calculation of phonon dispersions in semiconductors, *Phys. Rev., B* 43 (1991) 7231–7242.
- [22] R.M. Wentzcovitch, J.L. Martins, G.D. Price, Ab initio molecular dynamics with variable cell shape: application to MgSiO<sub>3</sub>, *Phys. Rev. Lett.* 70 (1993) 3947–3950.
- [23] D. Wallace, *Thermodynamics of Crystals*, Wiley, New York, 1972.
- [24] <http://www.pwscf.org>.
- [25] B. Hyde, S. Andersson, *Inorganic Crystal Structures*, Wiley, New York, 1989.
- [26] R.M. Wentzcovitch, N. Ross, G.D. Price, Ab initio study of MgSiO<sub>3</sub> and CaSiO<sub>3</sub> perovskites at lower-mantle pressures, *Phys. Earth Planet. Inter.* 90 (1995) 101–112.
- [27] P. Vinet, J.H. Rose, J. Ferrante, J.R. Smith, Universal features of the equation of state of solids, *J. Phys., Condens. Matter* 1 (1989) 1941–1963.
- [28] M. Wentzcovitch, L. Stixrude, B. Karki, B. Kiefer, *Geophys. Res. Lett.* 31 (2004) DOI: 10.1029/2004GL019704.
- [29] Y. Akahama, H. Kawamura, A.K. Singh, Equation of state of bismuth to 222 GPa and comparison of gold and platinum pressure scales to 145 GPa, *J. Appl. Phys.* 92 (2002) 5892–5897.
- [30] T. Tsuchiya, K. Kawamura, First-principles electronic thermal pressure of metal Au and Pt, *Phys. Rev., B* 66 (2002) 094115.
- [31] O.L. Anderson, D.G. Isaak, S. Yamamoto, Anharmonicity and the equation of state for gold, *J. Appl. Phys.* 65 (1989) 1534–1543.
- [32] J. Badro, G. Fiquet, F. Guyot, J.-P. Rueff, V.V. Struzhkin, G. Vankó, G. Monaco, Iron partitioning in earth's mantle: toward a deep lower mantle discontinuity, *Science* 300 (2003) 789–791.
- [33] Q. Williams, R. Jeanloz, Melting relations in the iron–sulfur system at ultra-high pressures: implications for the thermal state of the earth, *J. Geophys. Res.* 95 (1990) 19299–19310.
- [34] R. Boehler, Temperature in the earth's core from melting-point measurements of iron at high static pressures, *Nature* 363 (1993) 534–536.
- [35] M.J. Brown, T.J. Shankland, Thermodynamic parameters in the earth as determined from seismic profiles, *Geophys. J. R. Astron. Soc.* 66 (1981) 579–596.